JOURNAL OF GUIDANCE, CONTROL, AND DYNAMICS
Vol. 31, No. 1, January–February 2008

Minimum-Fuel Deployment for Spacecraft Formations via Optimal Control

Jean-Baptiste Thevenet* and Richard Epenoy†
Centre National d'Etudes Spatiales,
31401 Toulouse Cedex 9, France

DOI: 10.2514/1.30364

This paper focuses on the issue of minimum-fuel deployment for satellite formation flying. We address it as an optimal control problem, the necessary optimality conditions of which are derived from Pontryagin's maximum principle. These are numerically enforced by finding the root of a so-called shooting function. However, optimal control laws for minimum-fuel problems are discontinuous and produce shooting functions with singular Jacobian matrices. The resulting problems cannot be solved easily and require the use of a regularization technique. We extend our previously developed continuation-smoothing method to the multisatellite context by using an adapted initialization procedure. Because realistic mission scenarios may require it, our approach additionally offers the ability to slightly modify a given maneuver strategy to balance the fuel consumption among the satellites to a certain degree. A number of tests concerning low-Earth orbits are carried out in the paper as examples. Our model includes the J_2 effect, which leads to numerical difficulties. We show the efficiency of our method in this challenging context: several maneuver strategies are detected and analyzed from the space dynamics angle. We finally point out that beyond this application, a whole class of deployment/reconfiguration problems may be handled through this approach.

I. Introduction

USING small-satellite formations instead of a unique large-sized satellite is now considered as an interesting tradeoff for many space missions. The main advantages lie in lowering the missions costs while enhancing the performances. These missions give birth to new space mechanics challenges such as the fuel-optimal deployment problem that is considered in this paper. It consists in designing open-loop controls for each satellite that minimize the overall fuel expenditure while satisfying certain boundary conditions; the cluster will be placed from some injection conditions into a particular geometric configuration at a given final time. We will consider a spacecraft formation about an oblate Earth (the J_2 gravity term will be taken into account and other forces will be neglected).

This paper gives numerical examples concerning low-Earth orbits (LEO), but our method can also deal with highly elliptical orbit (HEO) problems. Indeed, due to the use of Gauss equations, it is possible to modify the dynamic model, including different kinds of perturbative forces. The method is also not restricted to deployment problems, but aims at solving reconfiguration issues; when the mission goals are modified, or after a satellite breakdown, computing optimal maneuvers is necessary to recover operational conditions. Nevertheless, even if the method is theoretically able to cope with different problems, it will have to be tested and tuned on each problem. It is indeed difficult to forecast its numerical behavior on a new problem.

Many contributions regarding formation flying of satellites are available. The envisioned problems, along with the proposed methods, are in very large numbers. We give a few references on this topic that will be classified according to the selected dynamics equations in the following sections.

First, several authors use linearized (Hill [1] and Clohessy and Wiltshire [2]) or time-varying linear (Lawden [3]) equations to describe the relative motion of the satellites within the formation. These equations are valid for short intersatellite distances only. In this case, the station-keeping or deployment problems may sometimes be provided with analytic solutions [4,5]. Yet, simplifying assumptions are then required, such as replacing the consumption criterion by an objective function of the energy type. Similarly, some prior knowledge of thrust history is needed. Without such assumptions, the minimum-fuel deployment problem has to be cast as an optimal control problem. So far, only numerical methods have turned out to be efficient in this context. Direct transcription methods are mostly used and proceed by discretizing the time horizon and the control and state variables accordingly. The optimal control and state discrete values are then computed by some numerical optimization method of either deterministic [6–8] or heuristic type (genetic algorithms, multi-agent optimization, planning, etc. [9–12]). These approaches are not only efficient, but also handle additional state constraints such as collision-avoidance requirements [7,8,13,14]. In [15], a mixed-integer linear programming approach is also developed with this aim in view.

Unfortunately, linear models become invalid when the intersatellite distances, the maneuver durations, or the J_2 effect are important. This motivates the use of general methods that can treat problems with nonlinear models.

As far as station-keeping is concerned, [16,17] provide sufficient conditions that yield J_2-invariant orbits (i.e., uncontrolled relative trajectories that do not drift apart). These results are of great importance for the formation design and the closed-loop control synthesis, but are not adapted to our purpose.

Let us now go back to deployment/reconfiguration problems for which nonlinear models such as Gauss equations are considered. We still may discretize the optimal control problem in this case and subsequently run some dynamic programming method (see [18], for instance). Nevertheless, our problems concern deployments that may last several weeks and with rapidly varying orbital parameters, due to J_2. The resulting program size is likely to be prohibitive. Consequently, alternative methods have to be envisioned such as in [19], in which an approach based upon the Hamilton–Jacobi–Bellman theory is developed. Our own indirect approach follows from the well-known Pontryagin maximum principle (PMP) [20],

Received 9 February 2007; revision received 23 July 2007; accepted for publication 2 August 2007.

*Postdoctoral Researcher, Orbital Maneuvers Department, 18 Avenue Edouard Belin; jbthevenet@yahoo.fr.

†Research Engineer, Orbital Maneuvers Department, 18 Avenue Edouard Belin; Richard.Epenoy@cnes.fr.

which states the necessary optimality conditions to be solved numerically. We will specialize this general scheme to the deployment problem.

The collision-avoidance problem will not be treated here, because the deployment strategies that were obtained from our tests did not reveal any collision risk. Obviously, collisions might occur in some other context, but we are not currently aware of any efficient way to tackle them via indirect methods. Indeed, taking into account the collision-avoidance requirement leads to adding a nonconvex state constraint to the initial problem, which is particularly complex to handle through PMP. Some authors [21] recommend an exterior penalty function method that forces the solution to satisfy the state constraint by the end of the algorithm. Unfortunately, it is known to produce ill-conditioned problems. Thus, we would rather go for an alternative approach that introduces artificial repulsive forces within the satellite dynamics [22]. Still, it is not clear how to give optimality certificates in this case and some further developments seem necessary, regardless of the method.

In addition to collision avoidance, our problem involves many difficulties. First, it is a nonconvex program with multiple local minima, each of them being related to a particular deployment strategy. Second, the minimum-fuel problem optimality conditions provide *bang-off-bang* controls and a nonsmooth shooting function. Consequently, a very good approximation of the solution is required for treating the two-point boundary-value problem (TPBVP) via a Newton-like method. Such an estimation is usually not available, and so an ad hoc approach will be needed. Furthermore, the short-period terms due to J_2 yield numerical errors and time consumption that increase as the deployment duration grows. Finally, the last major obstacle lies in the terminal conditions that mix the orbital parameters of the n satellites together. They prevent the deployment problem from being treated as n independent rendezvouses.

Consequently, we will adapt the continuation-smoothing method [23,24] to the multisatellite framework from previous studies on the monosatellite case. This will be done by developing a particular initialization process dedicated to the multisatellite case. In addition, the method will include a globalization technique devoted to finding as many solutions as possible and, potentially, to identify the global optimum among them. In addition, we will propose an original method that ensures a given distribution of the total propellant consumption among the satellites.

Our method does not aim at solving minimum-fuel deployments over a long period of time. Because of the use of nonlinear optimal control techniques, it is CPU-time-consuming and difficult to tune numerically when the deployment duration increases. In the same way, it is not clear how the method behaves when the number of satellites increases, although the computation time will be more important. Nevertheless, the main formation-flying missions that are envisioned today involve no more than six satellites, which should not cause failure of our method, as far as we know. If more satellites are to be accounted for, it is likely that some symmetry should exist within the formation, reducing the problem to a smaller one that could be handled by our approach.

In addition, our method does not take into account the combinatorial aspects of the deployment problem. The question is which satellite should be assigned to a given final position. In our application, this choice has very little influence on the global fuel consumption, because the satellites play a similar role (short initial intersatellite distances). In another context, the different combinations between initial and final positions should be tested to determine the best one. This could be done through the use of a combinatorial algorithm, for example.

Section II details the deployment optimal control problem and the difficulties it raises. We then develop, both theoretically and practically, the main features of our technique in Sec. III. The subsequent Sec. IV is dedicated to globalizing the method and balancing the fuel consumption among the satellites from an existing strategy. Finally, in Sec. V, we give some numerical results obtained in the LEO context that is described next.

II. Problem Statement

A. Notation

Let us consider a formation of n satellites (four in our application). The state vector x_j of equinoctial orbital parameters for the jth satellite S_j $(j = 1, \ldots, n)$ is defined according to

$$x_j = \begin{pmatrix} a_j \\ e_{x,j} = e_j \cos(\omega_j + \Omega_j) \\ e_{y,j} = e_j \sin(\omega_j + \Omega_j) \\ h_{x,j} = \tan(i_j/2)\cos(\Omega_j) \\ h_{y,j} = \tan(i_j/2)\sin(\Omega_j) \\ L_j = \omega_j + \Omega_j + v_j \end{pmatrix} \tag{1}$$

where $(a_j, e_j, i_j, \omega_j, \Omega_j, v_j)$ denotes the set of Keplerian osculating parameters for S_j.

Similarly, m_j stands for the mass of S_j $(j = 1, \ldots, n)$, $F_{\max}$ is the maximum thrust modulus of the engines, and I_{sp} is their specific impulse. Although in our application every satellite is supposed to be equipped with the same engine and to carry the same initial mass m_0, these conditions are not required for the method to properly work.

Furthermore, $x_{j,0}$ denotes the vector of initial orbital parameters for S_j $(j = 1, \ldots, n)$, g_0 stands for the acceleration due to gravity at sea level, and t_0 and t_f are the (fixed) initial and final dates, respectively. The control function (i.e., the normalized thrust vector for satellite S_j) is denoted by u_j $(j = 1, \ldots, n)$.

B. General Outline

The deployment problem that we consider involves four satellites, and among them, one is supposed to be a spare. The maneuver strategy for each satellite is sought such that the sum of the consumed masses is minimized and some boundary conditions are satisfied.

The deployment problem is cast as the following optimal control problem:

$$\begin{cases} \min J(u_1, \ldots, u_n) = -\sum_{j=1}^{n} m_j(t_f) \\ \dot{x}_j(t) = f[x_j(t)] + F_{\max} g[x_j(t)] \dfrac{u_j(t)}{m_j(t)} \\ \dot{m}_j(t) = -F_{\max} \dfrac{\| u_j(t) \|}{g_0 I_{\text{sp}}} \\ \| u_j(t) \| \leq 1 \;\; t \in [t_0, t_f] \qquad\qquad (j = 1, \ldots, n) \\ x_j(t_0) = x_{j,0} \;\; m_j(t_0) = m_0 \\ \psi_j[x_j(t_f)] = 0 \\ \phi[x_1(t_f), \ldots, x_n(t_f)] = 0 \end{cases} \tag{2}$$

Our application concerns LEO, and the Gauss equations associated with Eq. (1) are used to describe the motion of S_j $(j = 1, \ldots, n)$ in problem (2). The resulting dynamic model neglects the atmospheric drag, but takes into account the J_2 term of the Earth potential. This is of great importance because optimal trajectories (see Sec. V) should benefit from the J_2 effects, such as the differential drift in certain orbital parameters.

C. Terminal Conditions

Problem (2) includes the final conditions

$$\psi_j[x_j(t_f)] = 0 \qquad (j = 1, \ldots, n) \tag{3}$$

$$\phi[x_1(t_f), \ldots, x_n(t_f)] = 0 \tag{4}$$

First, some orbital parameters are explicitly set by Eq. (3) independently from one satellite to another. With $a_{j,f}$, $e_{x,j,f}$, $e_{y,j,f}$, and $i_{j,f}$ $(j = 1, \ldots, n)$ being given, the noncoupling final conditions of problem (2) take the form

$$\psi_j[x_j(t_f)] = \begin{bmatrix} a_j(t_f) - a_{j,f} \\ e_{x,j}(t_f) - e_{x,j,f} \\ e_{y,j}(t_f) - e_{y,j,f} \\ h_{x,j}(t_f)^2 + h_{y,j}(t_f)^2 - \tan^2\left(\frac{i_{j,f}}{2}\right) \end{bmatrix} \quad (j = 1, \ldots, n) \tag{5}$$

Thus, the final osculating values of semimajor axis and eccentricity are fixed for each satellite [$e_{x,j,f} = e_{y,j,f} = 0$ ($j = 1, \ldots, n$) in our application]. Similarly, the inclination value at $t = t_f$ is specified through the last component of $\psi_j[x_j(t_f)]$ in Eq. (5) (see expressions (1) of $h_{x,j}$ and $h_{y,j}$). Note that in our application, the targeted inclinations are identical: $i_{j,f} = i_f$ ($j = 1, \ldots, n$), where i_f is given.

Let us now focus on the additional constraint (4), The differences between the satellites at $t = t_f$ in some orbital parameters are actually fixed by Eq. (4), and ϕ is defined as

$$\phi[x_1(t_f), \ldots, x_n(t_f)] = \begin{bmatrix} \phi^1[x_1(t_f), x_2(t_f)] \\ \vdots \\ \phi^{n-1}[x_{n-1}(t_f), x_n(t_f)] \end{bmatrix} \tag{6}$$

In Eq. (6), every ϕ^j ($j = 1, \ldots, n-1$) relates to a pair of satellites $\{S_j, S_{j+1}\}$, and specifies, at the final date t_f, the corresponding differential values of the true longitude L and the right ascension of the ascending node Ω.

More precisely, for $j = 1, \ldots, n-1$,

$$\phi^j[x_j(t_f), x_{j+1}(t_f)] = \begin{bmatrix} h_{x,j}(t_f)h_{x,j+1}(t_f) + h_{y,j}(t_f)h_{y,j+1}(t_f) - \tan^2\left(\frac{i_f}{2}\right)\cos(\delta\Omega_{j,f}) \\ h_{x,j}(t_f)h_{y,j+1}(t_f) - h_{y,j}(t_f)h_{x,j+1}(t_f) - \tan^2\left(\frac{i_f}{2}\right)\sin(\delta\Omega_{j,f}) \\ \tan\left(\frac{L_{j+1}(t_f) - L_j(t_f)}{2}\right) - \tan\left(\frac{\delta L_{j,f}}{2}\right) \end{bmatrix} \tag{7}$$

where the constant $\delta\Omega_{j,f}$ stands for the difference in right ascension of the ascending node between S_j and S_{j+1} at $t = t_f$. Indeed, when $\phi^j[x_j(t_f), x_{j+1}(t_f)] = 0$, the first two equations combined with Eq. (1) imply that $\Omega_{j+1}(t_f) - \Omega_j(t_f) = \delta\Omega_{j,f}$. When two satellites S_j and S_{j+1} ($j \in \{1, \ldots, n-1\}$) are in the same plane at $t = t_f$, we have $\delta\Omega_{j,f} = 0$.

In an analogous manner, the constant $\delta L_{j,f}$ in Eq. (7) specifies the difference in true longitude at the final time between S_j and S_{j+1}. Note that the associated component of $\phi^j[x_j(t_f), x_{j+1}(t_f)]$ is defined through a tangent half-angle formula equivalent to $L_{j+1}(t_f) - L_j(t_f) = \delta L_{j,f}$ modulo 2π.

Let us finally underline that the constraint $\phi[x_1(t_f), \ldots, x_n(t_f)] = 0$ introduces coupling conditions between the state variables of problem (2). Thus, the n-satellite deployment problem will have to be treated as a whole.

Remark 1: As mentioned in the Introduction, the satellite assignment is not optimized here. More precisely, the choice of the final slot each satellite has to be placed into is not optimized [cf. Eqs. (5–7)]. In fact, this choice has very little influence on the global fuel consumption here, because the satellites play a similar role, due to their short initial interdistances (see Sec. V.A.2).

D. Optimal Bang-Off-Bang Controls

Hereafter, we apply PMP [20,25,26], the first-order necessary optimality condition for problem (2). Let us start by defining some notations that will be useful in the sequel.

Let us first collect the state variables into a $7n$-dimensional state vector $y(t)$. Let us then similarly define the costate vector $p_y(t)$ for problem (2), obtained by gathering the costates $p_{x_j}(t)$ and $p_{m_j}(t)$, associated with $x_j(t)$ and $m_j(t)$ ($j = 1, \ldots, n$), respectively. Finally, defining a multiple spacecraft $3n$-dimensional control vector $u(t)$, we have

$$y(t) = \begin{pmatrix} x_1(t) \\ \vdots \\ x_n(t) \\ m_1(t) \\ \vdots \\ m_n(t) \end{pmatrix}, \qquad p_y(t) = \begin{pmatrix} p_{x_1}(t) \\ \vdots \\ p_{x_n}(t) \\ p_{m_1}(t) \\ \vdots \\ p_{m_n}(t) \end{pmatrix}, \qquad u(t) = \begin{pmatrix} u_1(t) \\ \vdots \\ u_n(t) \end{pmatrix}$$

Now, due to the structure of problem (2), its Hamiltonian function can be written under the following form:

$$H[y(t), u(t), p(t)] = \sum_{j=1}^{n} H_j[x_j(t), m_j(t), u_j(t), p_{x_j}(t), p_{m_j}(t)]$$

such that for all $j = 1, \ldots, n$,

$$\begin{aligned} &H_j[x_j(t), m_j(t), u_j(t), p_{x_j}(t), p_{m_j}(t)] \\ &\quad = p_{x_j}(t)^T \left\{ f[x_j(t)] + F_{\max} g[x_j(t)] \frac{u_j(t)}{m_j(t)} \right\} \\ &\quad - F_{\max} p_{m_j}(t) \frac{\| u_j(t) \|}{g_0 I_{\text{sp}}} \end{aligned} \tag{8}$$

where the standard notation T denotes the transpose operator.

As a result, minimizing H with respect to $u(t)$ at fixed time t is equivalent to separately minimizing each $H_j[x_j(t), m_j(t), u_j(t), p_{x_j}(t), p_{m_j}(t)]$ with respect to $u_j(t)$ ($j = 1, \cdots, n$). The resulting optimal controls u_j^* ($j = 1, \ldots, n$) are then independent from one satellite to another. In the sequel, let $j \in \{1, \ldots, n\}$ be fixed.

According to [20,25,26], the optimal control function for satellite S_j is computed as

$$u_j^*(t) = \arg \min_{\|w\| \le 1} \left\{ -\frac{p_{m_j}(t)}{g_0 I_{\text{sp}}} \| w \| + p_{x_j}(t)^T g[x_j(t)] \frac{w}{m_j(t)} \right\} \quad t \in [t_0, t_1]$$

which leads to a bang-off-bang optimal control.

Indeed, if $g[x_j(t)]^T p_{x_j}(t) \neq \mathbf{0}_{3,1}$, Cauchy–Schwartz inequality states that

$$\begin{aligned} &-\frac{p_{m_j}(t)}{g_0 I_{\text{sp}}} \|w\| + p_{x_j}(t)^T g[x_j(t)] \frac{w}{m_j(t)} \\ &\quad \ge -\left(\frac{\| g[x_j(t)]^T p_{x_j}(t) \|}{m_j(t)} + \frac{p_{m_j}(t)}{g_0 I_{\text{sp}}} \right) \|w\| \quad \forall\ w | \|w\| \le 1 \end{aligned}$$

which turns into equality when vector w is collinear to $-g[x_j(t)]^T p_{x_j}(t)$.

Thus, using the switching function $\rho_j(t)$, defined as

$$\rho_j(t) = F_{\max} \left(\frac{\| g[x_j(t)]^T p_{x_j}(t) \|}{m_j(t)} + \frac{p_{m_j}(t)}{g_0 I_{\text{sp}}} \right) \tag{9}$$

the optimal control satisfies

1) if $g[x_j(t)]^T p_{x_j}(t) \neq \mathbf{0}_{3,1}$, $u_j^*(t)$ is given by

$$u_j^*(t) = -\beta_j(t) \frac{g[x_j(t)]^T p_{x_j}(t)}{\| g[x_j(t)]^T p_{x_j}(t) \|}$$

where $\beta_j(t)$ is the norm of $u_j^*(t)$ and is defined as

$$\beta_j(t) = \begin{cases} 0 & \text{if } \rho_j(t) < 0 \\ 1 & \text{if } \rho_j(t) > 0 \\ w \in [0,1] & \text{if } \rho_j(t) = 0 \end{cases} \tag{10}$$

2) if $g[x_j(t)]^T p_{x_j}(t) = \mathbf{0}_{3,1}$, $u_j^*(t)$ is such that

$$\|u_j^*(t)\| = \beta_j(t)$$

For all t, the thrust direction for S_j $(j = 1, \ldots, n)$ is given by vector $-g[x_j(t)]^T p_{x_j}(t)$ (unless $g[x_j(t)]^T p_{x_j}(t) = \mathbf{0}_{3,1}$). The sign of the switching function determines whether the thrust modulus is maximum or zero. This justifies the bang-off-bang terminology. The fact that $g[x_j(t)]^T p_{x_j}(t)$ is nonzero almost everywhere has to be checked when the problem is numerically being solved. In this case, the control will always be well-defined or, in other words, there will be no singular arc [25,26].

The differential equations governing the dynamics of $p_y(\cdot)$ on one hand and the transversality conditions between $p_y(t_f)$ and $y(t_f)$ on the other hand are given by PMP [20,25,26]. In particular, these transversality conditions define a so-called shooting function denoted by $\Phi(\cdot)$, with vector $z = p_y(t_0)$ as an unknown variable. The resulting system to be solved is then written as $\mathbf{\Phi(z)} = \mathbf{0}$. A modified Powell's hybrid method [27] that locally behaves like Newton's method will be used to this end.

E. Main Issues

Evaluating the shooting function $\Phi(\cdot)$ requires numerically solving $14n$ differential equations, including the costates dynamics. This task has to be performed many times and with a high level of accuracy, to find the roots of this function via Powell's method. Hence, it is essential to integrate the system both precisely and fast enough. This raises two main issues. First, the bang-off-bang structure of the controls u_j^* $(j = 1, \ldots, n)$ leads to a discontinuous right-hand side of the system. The eighth-order Runge–Kutta process with step-size control [28] hardly reaches the required level of accuracy in this context.

Second, the J_2 term induces short-period oscillations in the osculating-parameter history. The integration step size thus has to be reduced, and the amount of time needed to evaluate the shooting function increases as the number of revolutions gets high. This phenomenon limits the possible deployment duration for LEO applications.

Another major problem we have to face does not directly relate to integration aspects, but follows from the nonsmoothness of function $\Phi(\cdot)$. Indeed, the shooting function is not continuously differentiable and its Jacobian is singular on a large domain. Accordingly, Powell's algorithm may fail to converge to a solution of $\Phi(z) = 0$, and a specific technique such as the continuation-smoothing method [23] is required.

III. Continuation-Smoothing Method

A. Overview

The basic idea in [23] is to solve a sequence of auxiliary optimal control problems, the solutions of which converge toward a solution of the initial problem. More precisely, the method aims at finding a critical point (satisfying the PMP necessary optimality conditions) of each auxiliary problem, such as to build a sequence converging toward a critical point of the initial problem. The rationale here is to generate auxiliary problems with smooth optimal controls and regular associated shooting functions. In this context, Powell's method behaves well.

The auxiliary problem is obtained from problem (2) by adding to the objective function either a barrier or a penalty function term. The latter involves a function denoted by $F(\cdot)$ and is parameterized by a scalar $\epsilon > 0$ that will be driven to zero in the course of the iterations. The approach is referred to as a *penalty* method when $F(\cdot)$ takes finite values on $[0, 1]$, and as a *barrier* method when $F(w) \to -\infty$ as w approaches zero or one.

Consider the following problem:

$$\begin{cases} \min J_\epsilon(u) = -\sum_{j=1}^n \left\{ m_j(t_f) + \epsilon \int_{t_0}^{t_f} F[\| u_j(t) \|] \, \mathrm{d}t \right\} \\ \dot{x}_j(t) = f[x_j(t)] + F_{\max} g[x_j(t)] \dfrac{u_j(t)}{m_j(t)} \\ \dot{m}_j(t) = -F_{\max} \dfrac{\| u_j(t) \|}{g_0 I_{\mathrm{sp}}} \\ \| u_j(t) \| \le 1 \;\; t \in [t_0, t_f] \qquad (j = 1, \ldots, n) \\ x_j(t_0) = x_{j,0} \;\; m_j(t_0) = m_0 \\ \psi_j[x_j(t_f)] = 0 \\ \phi[x_1(t_f), \ldots, x_n(t_f)] = 0 \end{cases} \tag{11}$$

The continuation process starts by first solving problem (11) for an initial value of ϵ (say, ϵ_1). Then, defining a decreasing sequence of values taken by ϵ ($\epsilon_1 > \epsilon_2 > \cdots > \epsilon_N$), problems (11) associated with $\epsilon = \epsilon_k$ $(k = 2, \ldots, N)$ are successively solved by using the solution obtained at step $(k-1)$ as an initial guess for the current step k (see [23]). The process stops when the desired accuracy on the objective function ϑ is reached, for some index k:

$$|J_{\epsilon_{k+1}}(u^*_{\epsilon_{k+1}}) - J_{\epsilon_k}(u^*_{\epsilon_k})| \le \vartheta, \qquad \vartheta > 0 \tag{12}$$

where $u^*_{\epsilon_k}$ denotes the optimal control vector for problem (11) associated with $\epsilon = \epsilon_k$.

Remark 2: The convergence proof of the method is not given here because it was established in the monosatellite case [23]. The extension to the multisatellite framework is straightforward. Hence, we limit ourselves to practically checking the convergence of the algorithm on the n-satellite problem considered here.

Remark 3: Each optimal control $u^*_{\epsilon,j}$ $(j = 1, \ldots, n)$ associated with problem (11) only depends upon the state x_j and the costate p_{x_j}, and so the controls remain independent of one another.

B. Penalty/Barrier Functions

This section examines two instances of the function F that will be used next. For a given value of ϵ, the optimal controls $u^*_{\epsilon,j}$ associated with the satellite S_j $(j = 1, \ldots, n)$ will be derived in both cases.

Let us first consider the following penalty-type quadratic function:

$$F^1(w) = w(1-w) \ge 0 \quad \forall \; w \in [0,1] \tag{13}$$

Applying PMP to the corresponding problem (11) yields the following optimal control $u^*_{\epsilon,j}$ associated with S_j $(j = 1, \ldots, n)$:

1) If $g[x_j(t)]^T p_{x_j}(t) \neq \mathbf{0}_{3,1}$,

$$u^*_{\epsilon,j}(t) = -\beta_{\epsilon,j}(t) \frac{g[x_j(t)]^T p_{x_j}(t)}{\| g[x_j(t)]^T p_{x_j}(t) \|} \tag{14}$$

Consequently, $u^*_{\epsilon,j}$ and u^*_ϵ are similarly defined as for the thrust direction. However, the control norm is modified according to

$$\beta_{\epsilon,j}(t) = \begin{cases} 0 & \text{if } \rho_j(t) \le -\epsilon \\ 1 & \text{if } \rho_j(t) \ge \epsilon \\ \frac{1}{2} + \frac{\rho_j(t)}{2\epsilon} & \text{if } \rho_j(t) \in [-\epsilon, \epsilon] \end{cases}$$

where ρ_j is given by Eq. (9).

2) If $g[x_j(t)]^T p_{x_j}(t) = \mathbf{0}_{3,1}$, $u^*_{\epsilon,j}(t)$ is of any direction but satisfies

$$\| u^*_{\epsilon,j}(t) \| = \beta_{\epsilon,j}(t)$$

Let us now fix $t \in [t_0, t_f]$ and $j \in \{1, \ldots, n\}$. It is clear that as functions of $\rho_j(t)$ 1) the control norm $\beta_{\epsilon,j}$ converges to β_j when $\epsilon \to 0$ and 2) $u^*_{\epsilon,j}$ is continuous, but nondifferentiable for $\rho_j(t) = \pm\epsilon$.

Thus, a continuous but non-C^1 control function was obtained. In addition, as a function of $\rho_j(t)$ (t being fixed), it converges to the optimal control function of the initial problem (2).

Let us now turn to our alternative (barrier-type logarithmic) function F, defined by

$$F^2(w) = \log(w) + \log(1-w) \quad \forall\ w \in]0,1[\tag{15}$$

Let us first notice that the control norm is constrained here to stay in the interval $]0,1[$.

Here, the optimal controls given by PMP are similar to those in Eq. (14), as soon as $g[x_j(t)]^T p_{x_j}(t) \neq \mathbf{0}_{3,1}$. In this case, the norm of $u^*_{\epsilon,j}(t)$ $(j = 1,\ldots,n)$ is defined as

$$\beta_{\epsilon,j}(t) = \frac{2\epsilon}{2\epsilon - \rho_j(t) + \sqrt{\rho_j(t)^2 + 4\epsilon^2}}$$

Conversely, when $g[x_j(t)]^T p_{x_j}(t) = \mathbf{0}_{3,1}$, the thrust direction is free and we only have

$$\| u^*_{\epsilon,j}(t) \| = \beta_{\epsilon,j}(t)$$

Let t be temporarily fixed again; $\beta_{\epsilon,j}$ $(j = 1,\ldots,n)$ is now a C^∞ function of $\rho_j(t)$ that approximates to β_j as $\epsilon \to 0$. The corresponding optimal control function is smooth enough to efficiently use Powell's method.

C. Implementation

The preceding section underlined the importance of smoothing the control function to guarantee Powell's method convergence. The next section addresses implementation aspects.

1. *Parameter Update Rules*

Powell's method efficiency not only requires smooth functions, but also a good estimate of the sought solution. This means that some adequate initial guess must be provided every time that the TPBVP has to be solved (i.e., for every value ϵ_k of ϵ).

At the current stage k of the algorithm, let $\Phi_{\epsilon_k}(z) = 0$ denote the system to be solved; $z^*_{\epsilon_{k-1}}$ denotes the solution obtained at stage $k-1$, and z_{0,ϵ_k} denotes the initial guess of the current solution. As a general rule, the solution obtained at the previous stage will be used as the initial guess for the new problem: $z_{0,\epsilon_k} = z^*_{\epsilon_{k-1}}$.

In case of failure, a new value of ϵ will be picked in $]\epsilon_k, \epsilon_{k-1}[$ and the process possibly renewed even if it means producing a slowly decreasing sequence $(\epsilon_k)_{k\in\mathbb{N}}$. The rationale here is that if for some k, the ratio $r_k = \epsilon_k/\epsilon_{k-1}$ is sufficiently close to one, the previous optimal solution necessarily lies in Powell's method attraction basin for the new problem.

In practice, the sequence $(r_k)_{k\in\mathbb{N}}$ usually reaches a stable value $r \in]0,1[$ after a few iterations. Finally, when initializing the algorithm, the question of how to choose z_{0,ϵ_1} arises.

2. *Initial Phase: Continuation on the Terminal Conditions*

Hereafter, we propose an original method for properly initializing the algorithm. To this end, we first perform a numerical integration of the state dynamics over the deployment duration from the initial conditions in problem (2) and with disabled controls:

$$u_j(t) = 0 \qquad (j = 1,\ldots,n) \quad \forall\ t \in [t_0, t_f]$$

We obtain the value of the state variables at $t = t_f$, denoted by $\overline{x_j}(t_f)$ $(j = 1,\ldots,n)$, that correspond to a natural drift of the satellites under the influence of J_2. We may then evaluate the violation of the terminal constraints as

$$\overline{\psi_{j,f}} = \psi_j[\overline{x_j}(t_f)] \neq 0 \qquad (j = 1,\ldots,n)$$
$$\overline{\phi_f} = \phi[\overline{x_1}(t_f),\ldots,\overline{x_n}(t_f)] \neq 0$$

Let us now consider the following problem parameterized by $\lambda \in [0,1]$:

$$\begin{cases} \min J_{\epsilon_0}(u) = -\sum_{j=1}^n \left\{ m_j(t_f) + \boldsymbol{\epsilon_0} \int_{t_0}^{t_f} \mathbf{F^1}[\| u_j(t) \|]\,\mathrm{d}t \right\} \\ \dot{x}_j(t) = f[x_j(t)] + F_{\max} g[x_j(t)] \dfrac{u_j(t)}{m_j(t)} \\ \dot{m}_j(t) = -F_{\max} \dfrac{\| u_j(t) \|}{g_0 I_{\mathrm{sp}}} \\ \| u_j(t) \| \leq 1 \ t \in [t_0, t_f] \qquad (j = 1,\ldots,n) \\ x_j(t_0) = x_{j,0} \ m_j(t_0) = m_0 \\ \psi_j[x_j(t_f)] = \boldsymbol{\lambda}\, \overline{\psi_{j,f}} \\ \phi[x_1(t_f),\ldots,x_n(t_f)] = \boldsymbol{\lambda}\, \overline{\phi_f} \end{cases} \tag{16}$$

where initially $\lambda = 1$ and

$$\epsilon_0 = \frac{F_{\max}}{g_0 I_{\mathrm{sp}}}$$

This problem results from problem (11), with modified final conditions and a particular instance $[\epsilon_0, F^1(\cdot)]$ of the pair $[\epsilon, F(\cdot)]$ [cf. Eq. (13)].

In addition, noticing that for all $j = 1,\ldots,n$,

$$\begin{aligned} -m_j(t_f) &= \frac{F_{\max}}{g_0 I_{\mathrm{sp}}} \int_{t_0}^{t_f} \| u_j(t) \| \,\mathrm{d}t - m_j(t_0) \\ &= \epsilon_0 \int_{t_0}^{t_f} \| u_j(t) \| \,\mathrm{d}t - m_j(t_0) \end{aligned}$$

we conclude that the criterion in problem (16) reduces to the quadratic function

$$\epsilon_0 \sum_{j=1}^n \left\{ \int_{t_0}^{t_f} \|u_j(t)\|^2 \,\mathrm{d}t \right\}$$

up to an additive constant. Consequently, the problem (16) associated with $\boldsymbol{\lambda} = 1$ has, by construction, the vector-valued function:

$$u^*_{\epsilon_0}(t) = \begin{pmatrix} u^*_{\epsilon_0,1}(t) \\ \vdots \\ u^*_{\epsilon_0,n}(t) \end{pmatrix}$$

where $\boldsymbol{u^*_{\epsilon_0,j}(t)} = 0$ $(j = 1,\ldots,n)$ $\forall\ t \in [t_0, t_f]$ for a global solution.

In addition, by applying PMP to this problem, it can be shown that the following vector

$$p_y(t_0) = \begin{pmatrix} \mathbf{0}_{6n,1} \\ -\mathbf{1}_{n,1} \end{pmatrix} \tag{17}$$

would be a zero of the corresponding shooting function, if a Keplerian model was used. Our application takes J_2 into account, and so this condition is not satisfied. Still, the norm of the shooting function at $z = p_y(t_0)$ given by Eq. (17) remains negligible, and the vector (17) may be considered as a very good approximation of the solution of problem (16), with $\lambda = 1$.

In short, we modify problem (11) by first adding a nonzero right-hand side to the final conditions, then choosing a particular value of ϵ and a specific (quadratic) function F, to be able to provide a solution to the problem.

We still need to perform a continuation phase on the right-hand side of the final conditions: a sequence of problems (16) associated with values λ_k of λ are successively solved with $\lambda_k \to 0$. At every step, the solution of problem $(k-1)$ is used as an initial guess of the current problem k, associated with λ_k. As before, failure cases may occur, inducing a slowing down of the decrease of $(\lambda_k)_k$.

Eventually, when problem (16) is solved for $\lambda = 0$, a zero of the shooting function associated with problem (11) and denoted by $z^*_{\epsilon_0}$ is available. From then on, it would seem natural to free ϵ, for which the value was frozen at ϵ_0 until now, and to decrease it toward zero. This

would enable us to approach the bang-off-bang solution following the outline described in Sec. III.A. However, numerical issues quickly appear if the continuation technique is carried out with the quadratic penalty function F^1. This follows from the local nondifferentiability of the associated optimal controls (cf. Sec. III.B).

As a result, it is necessary to switch to a function that gives smoother optimal controls such as F^2 [cf. Eq. (15)]. In [23], it was shown in the monosatellite case how an appropriate value of ϵ might be computed, in the sense that $z^*_{\epsilon_0}$ would be a good estimate of the solution of problem (11) with F^2. We denote such a value by ϵ_1, in accordance with Sec. III.A. The method that is used in our algorithm is absolutely identical, and so we refer the reader to [23] for details.

Once this value has been computed, problem (11) is solved with $[\epsilon, F(\cdot)] = [\epsilon_1, F^2(\cdot)]$ and $z_{0,\epsilon_1} = z^*_{\epsilon_0}$ as a starting point. The continuation process on ϵ is then run for the logarithmic barrier F^2 until satisfaction of the termination criterion (12).

IV. Additional Features

A. Globalization Technique

First, recall that problem (2) is nonconvex and that PMP is a first-order necessary optimality condition that only yields critical points of the problem in this case (minima, maxima, or saddle points). Thus, our implementation includes an additional algorithmic level dedicated to locate as many solutions (critical points) of our problem as possible. With this end in view, a set of initial unknown costate vectors that will be named *candidates* are randomly generated at a given stage of the previously described algorithm. Then our (local) continuation-smoothing method is carried on from each of the candidates. It is hoped that they will eventually provide distinct maneuver strategies.

However, we recall that providing a good initial guess of the optimal costate is decisive for Powell's method. Accordingly, fully random candidates are not satisfactory, and the process will be performed by slightly disturbing the currently nominal vector z^*_ϵ, for some ϵ. A tradeoff has to be made here, because at the same time, the distance from the candidates to z^*_ϵ has to be large enough to avoid convergence to the same solution.

Several phases of the algorithm or, equivalently, several values of ϵ may be envisioned as a starting point for this process. Our numerical tests suggest that it has to be activated after the first iteration of the continuation on ϵ for F^2; that is, for $\epsilon = \epsilon_1$. So the vector $z^*_{\epsilon_1}$ is perturbed to obtain candidates from which as many continuation schemes are operated on.

If the process had been started earlier (say, from the kth step of the initial phase in Sec. III.C.2), then it would have been necessary to run all its remaining stages from each candidate. This would have been much too time-consuming.

Conversely, the random process might have been activated at the very end of the algorithm. This strategy was given up because the controls are nonsmooth for ϵ close to zero. Hence, Powell's method becomes highly sensitive in this case and often fails to converge.

This heuristic is not guaranteed to find the global minimum of the problem. It is usually neither able to produce the comprehensive set of critical points nor to prove that they are minima or maxima. Yet it enables, in practice, to efficiently generate several solutions. The corresponding deployment strategies differ in the directions and dates of thrust, as well as in the overall consumed propellant mass and the way it is balanced among the satellites.

B. Balancing the Consumptions

This section is devoted to a technique that brings an existing deployment strategy to finally satisfy a balance condition on the fuel consumption among the satellites.

1. Modeling

Ideally, problem (2) should be altered by adding the following constraint:

$$\gamma[m_1(t_f), \ldots, m_n(t_f)] \leq 0 \tag{18}$$

where $\gamma(\cdot)$ is defined for a given deployment strategy according to

$$\gamma[m_1(t_f), \ldots, m_n(t_f)] = \max_{1\leq k<j\leq n} |m_j(t_f) - m_k(t_f)| - \overline{\gamma} \sum_{j=1}^{n} [m_0 - m_j(t_f)] \tag{19}$$

for a fixed $\overline{\gamma} \in [0, 1]$.

Thus, the maximum difference

$$\Delta m_{\max} = \max_{1\leq k<j\leq n} |m_j(t_f) - m_k(t_f)|$$

among the satellites consumptions would be bounded above by a fraction $\overline{\gamma}$ of their sum

$$c = \sum_{j=1}^{n} [m_0 - m_j(t_f)]$$

However, Eq. (18) is nonsmooth and, as a result, cannot be directly handled through PMP.

Hence, we will use the following constraint instead:

$$\theta[m_1(t_f), \ldots, m_n(t_f)] \geq \overline{\theta} \tag{20}$$

where $\overline{\theta} \in [0, 1]$ and $\theta(\cdot)$ is defined for a given deployment strategy according to

$$\theta[m_1(t_f), \ldots, m_n(t_f)] = \frac{-\sum_{j=1}^{n} \zeta_j \log \zeta_j}{\log(n)} \tag{21}$$

where

$$\zeta_j = \left(\frac{m_j(t_f)}{\sum_{k=1}^{n} m_k(t_f)} \right) \qquad (j = 1, \ldots, n) \tag{22}$$

Remark 4: In the sequel, $\boldsymbol{P}_{\bar{\theta}_{\geq}}$ will denote problem (2) combined with the additional constraint (20) and $\boldsymbol{P}_{\bar{\theta}_{=}}$ will denote problem (2) combined with the equality constraint $\theta[m_1(t_f), \ldots, m_n(t_f)] = \bar{\theta}$.

Our purpose is then to solve problem $\boldsymbol{P}_{\bar{\theta}_{\geq}}$. Let us now clarify this choice.

First, notice that ζ_j $(j = 1, \ldots, n)$, defined by Eq. (22), stays in the interval $]0, 1[$. Hence, the entropy function involved in Eq. (21),

$$-\sum_{j=1}^{n} \zeta_j \log \zeta_j$$

with

$$\sum_{j=1}^{n} \zeta_j = 1$$

takes its values in $]0, \log(n)]$. Then it can be shown quite easily that its maximum, $\log(n)$, is reached at

$$\hat{\zeta}_j = \tfrac{1}{n} \qquad (j = 1, \ldots, n)$$

(i.e., when exactly the same propellant mass has been consumed by every satellite). The same goes for $\theta(\cdot)$, which reaches its maximum $\hat{\theta} = 1$ at the same time. Conversely, a sufficient condition to get a perfect distribution $\theta[m_1(t_f), \ldots, m_n(t_f)] = \hat{\theta}$ is to impose $\bar{\theta} = 1$ in Eq. (20).

Second, when $\bar{\theta} = 0$, constraint (20) is always satisfied. This amounts to saying there is no constraint anymore.

As a conclusion, any solution satisfying Eq. (20) for a given $\bar{\theta} \in]0, 1[$ ensures a consumption balance degree among the satellites that is superior to that defined by $\bar{\theta}$.

Remark 5: As for constraint (18), fixing $\bar{\gamma} = 0$ leads to a perfect balance, whereas $\bar{\gamma} = 1$ amounts to relaxing the constraint. Moreover, for values in $]0, 1[$, it is not possible to strictly associate a value of $\gamma[m_1(t_f), \ldots, m_n(t_f)]$ with $\theta[m_1(t_f), \ldots, m_n(t_f)]$. Finally,

notice that with $\theta(\cdot)$ being a C^∞ function of $m_j(t_f)$ $(j = 1, \cdots, n)$, Eq. (20) is well-adapted to PMP.

2. Balance Constraint Implementation

Observing that Eq. (20) is the only constraint in $P_{\bar{\theta},\geq}$ of the inequality type, we are going to replace it by an equality constraint that is best adapted to PMP.

First, we know from optimization theory that

Theorem 1: Any critical point (solution of the PMP conditions) of problem (2) satisfying Eq. (20) (respectively, $\theta[m_1(t_f), \ldots, m_n(t_f)] = \bar{\theta}$) is also a critical point of $P_{\bar{\theta},\geq}$ (respectively, $P_{\bar{\theta},=}$).

If problem (2) were a convex problem [as well as $P_{\bar{\theta},\geq}$ in this case, because $\theta(\cdot)$ is a concave function], we would have the following results:

1) Any critical point of problem (2) is a global minimum.

2) If the global minima of problem (2) satisfy $\theta[m_1(t_f), \ldots, m_n(t_f)] < \bar{\theta}$, then the global minima of $(P_{\bar{\theta},\geq})$ necessarily satisfy $\theta[m_1(t_f), \ldots, m_n(t_f)] = \bar{\theta}$.

From these observations, we build a method that modifies a solution of the problem (2), so that it eventually satisfies the balance constraint (20). Section IV.B.3 will ultimately discuss whether it is optimal toward $P_{\bar{\theta},\geq}$, as initially sought.

Now let z be a critical point of problem (2) associated with $\theta[m_1(t_f), \ldots, m_n(t_f)] = \theta_0$. Two cases are considered: 1) $\theta_0 \geq \bar{\theta}$; in this case, we know from Theorem 1 that z is also a critical point of $P_{\bar{\theta},\geq}$ and 2) $\theta_0 < \bar{\theta}$, a critical point of $P_{\bar{\theta},=}$, is sought by modifying z so that $\theta[m_1(t_f), \ldots, m_n(t_f)]$ increases until $\bar{\theta}$. Thus, we use a continuation process dedicated to finding a critical point of $P_{\eta,=}$, with η ranging from θ_0 to $\bar{\theta}$. As seen from Theorem 1, z is also a critical point of $P_{\theta_0,=}$ and the continuation on η would allow finally discovering a critical point of $P_{\bar{\theta},=}$. Numerical issues arise again if the preceding process is carried out trying to solve each $P_{\eta,=}$ $(\eta \in [\theta_0, \bar{\theta}])$ through the continuation-smoothing method, up to ϵ close to zero. This suggests starting the continuation process at a greater ϵ value, when controls are smoother. To remain concise, we will not go further into details with this aspect of the process.

3. Optimality Concerns

Because problem (2) is nonconvex, the preceding items 1 and 2 are not true. So a critical point of $P_{\bar{\theta},=}$ is obtained by the process previously described, but we cannot guarantee to have found a local minimum of $P_{\bar{\theta},=}$ or a local minimum of $P_{\bar{\theta},\geq}$. We have simply modified a given maneuver strategy to satisfy $\theta[m_1(t_f), \ldots, m_n(t_f)] = \bar{\theta}$.

Nevertheless, when the preceding process starts from a critical point z that is a local minimum of problem (2), we may hope that it converges to a local minimum of $P_{\bar{\theta},=}$ and $P_{\bar{\theta},\geq}$ as soon as $\bar{\theta}$ is sufficiently close to θ_0. In this case, indeed, because problem (2) is convex in the vicinity of z, our local continuation process normally yields a sequence of solutions (remaining close to z) that converges to the closest local minimum of $P_{\bar{\theta},=}$. The last solution is also a local minimum of $P_{\bar{\theta},\geq}$ in this case, due to the local convexity of problem (2).

V. Numerical Examples

This section presents some numerical results obtained by our method on the LEO deployment problem described in Sec. II. Recall that it may easily be transposed into a different context by modifying the dynamic equations and the boundary conditions in problem (2).

A. Deployment Data

1. Shared Parameters

a. Initial Conditions. The four satellites are injected at $t = t_0 = 0.0$ s into the same heliosynchronous orbit:

$$(a_j, e_j, i_j, \omega_j, \Omega_j)^T(t_0) = (a_0, e_0, i_0, \omega_0, \Omega_0)^T \qquad (j = 1, \ldots, n) \tag{23}$$

where $a_0 = 7029.48$ km, $e_0 = 1.27 \times 10^{-3}$, $i_0 = 98.08$ deg, $\omega_0 = 214.51$ deg, $\Omega_0 = 209.80$ deg, initial masses are identical (see Sec. II.B) and so $m_j(t_0) = m_0$ $(j = 1, \ldots, n)$, with $m_0 = 120$ kg.

According to the notation defined in Sec. II.B, we also take $F_{\max} = 4$ N and $I_{sp} = 210$ s.

b. Final Conditions. At $t = t_f$, the following targeted parameters are shared by the four satellites:

$$(a_{j,f}, e_{j,f}, i_{j,f})^T = (a_f, e_f, i_f)^T \qquad (j = 1, \ldots, n) \tag{24}$$

where $a_f = 7031$ km, $e_f = 0$, and $i_f = 98.08$ deg.

2. Specific Parameters

a. Initial Configuration. Initially, the satellites are spread along the orbit described in Sec. V.A.1, two successive satellites being dephased by 0.016 deg (2 km distant). More precisely, for $(j = 1, \ldots, n)$, the true anomaly v_j of the satellite S_j satisfies $v_j(t_0) = v_{j,0}$, with $v_{1,0} = 209.5601$ deg, $v_{2,0} = 209.5764$ deg, $v_{3,0} = 209.5438$ deg, and $v_{4,0} = 209.5275$ deg.

This configuration is illustrated by Fig. 1. The satellites are sorted out along the orbit in such a way that the collision risk is minimized during the deployment phase toward the final configuration, described next. However, this has very little influence on the maneuver strategies and the corresponding consumptions. The satellites play a similar role, the initial intersatellite distances being negligible when compared with the final distances.

b. Final Configuration. The final differences in right ascension of the ascending node and true longitude are fixed to the following values, in accordance with the previous notation (cf. Sec. II.C): $\delta\Omega_{1,f} = 0.0$ deg, $\delta\Omega_{2,f} = +0.47$ deg, and $\delta\Omega_{3,f} = 0.0$ deg on one hand, and

$\delta L_{1,f} = +0.41$ deg, $\delta L_{2,f} = -0.14$ deg, and $\delta L_{3,f} = -0.41$ deg on the other hand.

Instead of the true longitude, we now express these conditions in terms of the true latitude argument $\alpha = \omega + v$, so that the forthcoming results might be more easily interpreted: $\alpha_2(t_f) - \alpha_1(t_f) = \delta\alpha_{1,f} = 0.41$ deg, $\alpha_3(t_f) - \alpha_2(t_f) = \delta\alpha_{2,f} = -0.61$ deg, $\alpha_4(t_f) - \alpha_3(t_f) = \delta\alpha_{3,f} = -0.41$ deg, with $\delta\alpha_{j,f} = \delta L_{j,f} - \delta\Omega_{j,f}$ $(j = 1, \ldots, n-1)$.

As shown in Fig. 2, satellites S_1 and S_2 are placed into the same orbit as S_3 and S_4, respectively $(\delta\Omega_{1,f} = \delta\Omega_{3,f} = 0.0$ deg). In addition, the equality $\delta\alpha_{3,f} = -\delta\alpha_{1,f}$ implies that the distance d between S_3 and S_4 is equal to that between S_1 and S_2 (neglecting short-period oscillations due to J_2), with $d = 50$ km, the final orbits being circular with the same radius. Once the final configuration has

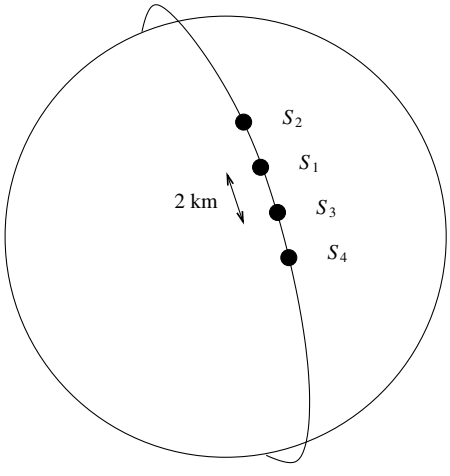

Fig. 1 Initial configuration.

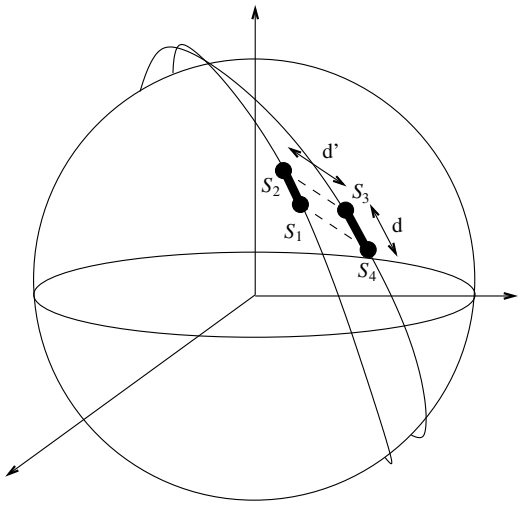

Fig. 2 Final configuration.

been established, the formation geometry in Fig. 2 varies along the orbit, but the targeted differences in α and Ω force the distance d' to remain close to 100 km.

From a space mechanics point of view, the expensive part of the maneuvers concerns the separation of the planes containing S_1 and S_2 on one hand and S_3 and S_4 on the other hand. Indeed, the other parameters (semimajor axis, eccentricity, and inclination) undergo very few changes from the initial to final dates, except for the true latitude argument. However, the targeted differences in α will be easily obtained via some small tangential maneuvers. Therefore, we will mainly focus in the sequel on the differential parameters between S_2 and S_3 (which is equivalent to considering S_1 and S_4).

B. Deployment over Seven Days

We now exhibit two deployment strategies computed by our algorithm for $t_f = 7$ days. The globalization technique (see Sec. IV.A) has successfully located seven deployment strategies (cf. Table 1), corresponding to an overall fuel consumption ranging from 10.62 kg (worst) to 6.58 kg (best). The latter will be referred to as the *global solution* in the sequel, though we cannot prove that it is actually the global one.

Let us first introduce some notation that will be useful to the analysis of the strategies found by our method. We denote $(X_j - X_i)_m$ as the time-averaged difference in orbital parameter X between satellites S_i and S_j over the deployment:

Table 1 Consumption and distribution features

sol	c, kg	$(1-\theta)$	$\Delta m_{\max}$, kg	$(\Delta m_{\max}/c) \times 100$
1	10.62	2.0×10^{-6}	5.83×10^{-1}	5.5
2	8.84	1.7×10^{-5}	1.97	22
3	8.54	7.5×10^{-5}	4.06	48
4	7.34	1.4×10^{-11}	1.61×10^{-3}	0.02
5	7.12	1.5×10^{-7}	1.60×10^{-1}	2.2
6	7.05	1.2×10^{-7}	1.38×10^{-1}	2.0
7	6.58	4.7×10^{-8}	8.61×10^{-2}	1.3
32	8.72	1.7×10^{-5}	1.88	22

Table 2 Evolution of the differential parameters versus t_f

t_f, days	c, kg	$(a_3 - a_2)_m$ m	$(i_3 - i_2)_m$, deg	$[(\Omega_3 - \Omega_2)_d]/\delta\Omega_{2,f} \times 100$
3.5	6.99	175	0.048	4.5
7	6.58	90	0.084	14.7
14	5.49	55	0.115	41.5
16.5	5.23	50	0.114	49.0
19	4.78	40	0.115	56.6

$$(X_j - X_i)_m = \frac{1}{t_f}\int_0^{t_f} [X_j(t) - X_i(t)]\,\mathrm{d}t$$

1. Global Solution

The sum of the satellite consumptions here amounts to 6.58 kg through 27 maneuvers. According to Fig. 3, the strategy that is used here to obtain the targeted difference in Ω at $t = t_f$ ($\delta\Omega_{2,f} = 0.47$ deg) between S_2 and S_3, combines the two following effects:

1) The differential drift in Ω, due to J_2, that relates to an inclination difference between the orbits $(i_3 - i_2)_m$ (amounting to $\Delta i_{\delta\Omega_{2,f}} = +0.08$ deg) caused by out-of-plane and opposed thrusts on both satellites.

2) The instantaneous effect on Ω is due to the same out-of-plane thrusts (located at both beginning and end of the deployment).

In addition, the existence of a semimajor axis difference $(a_3 - a_2)_m$ enables creating a difference in the true latitude argument $\delta\alpha_{2,f} = -0.61$ deg at $t = t_f$. The corresponding value $\Delta a_{\delta\alpha_{2,f}} = +90$ m may be seen in Fig. 3.

Figure 4 gives similar graphics concerning S_1 and S_2. Again, a slight semimajor axis difference $(a_2 - a_1)_m$ was produced to

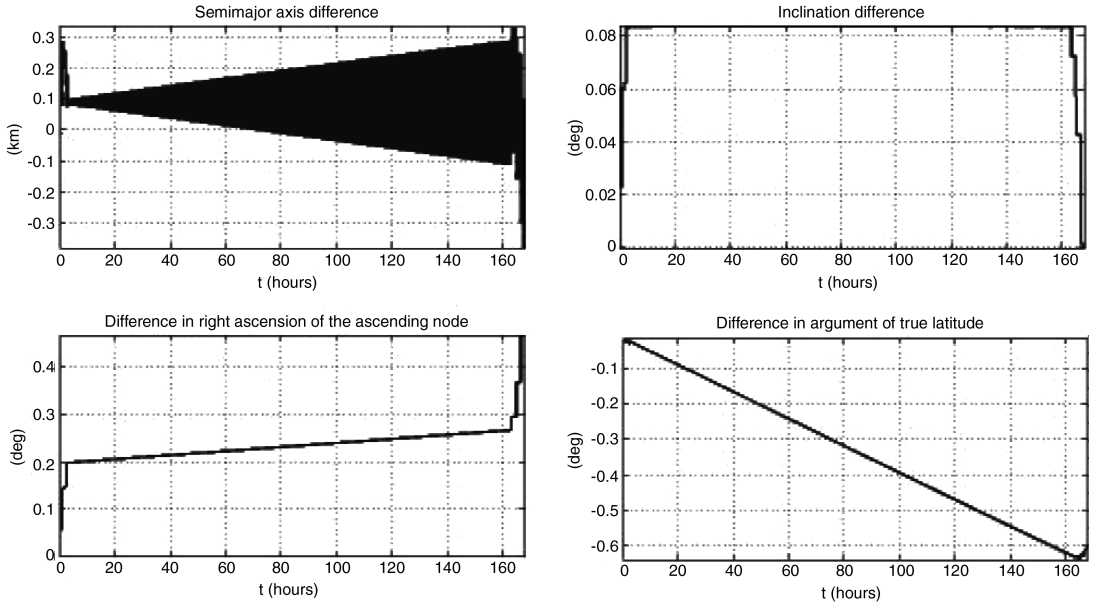

Fig. 3 Time evolution of the differential parameters between satellites S_2 and S_3; global solution.

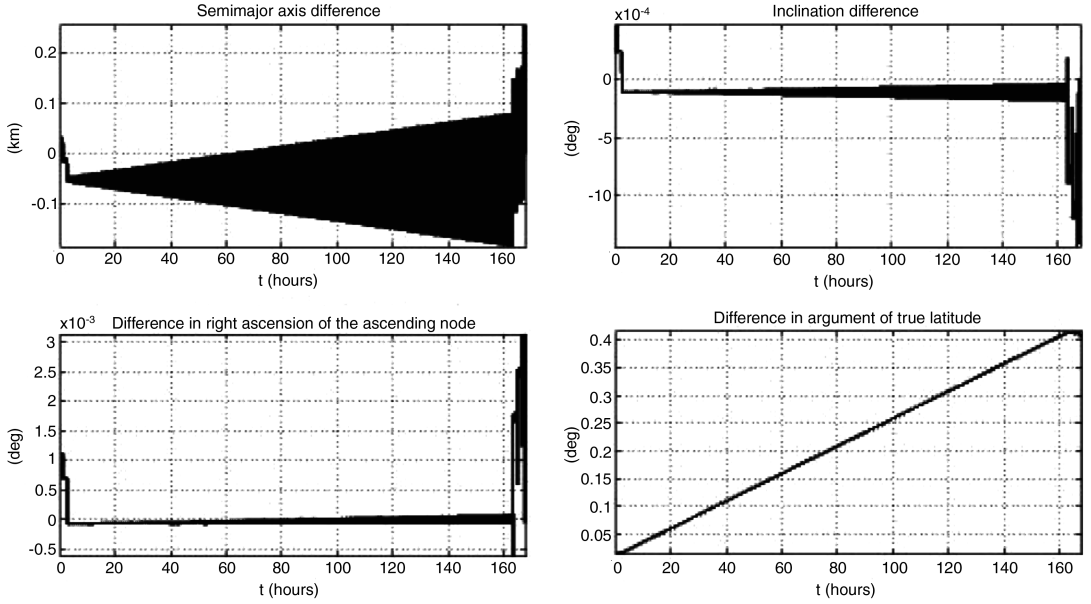

Fig. 4 Time evolution of the differential parameters between satellites S_1 and S_2; global solution.

dephase the satellites at final time t_f; that is, to obtain $\delta\alpha_{1,f} = +0.41$ deg. Its value is estimated to be $(a_2 - a_1)_m \approx \Delta a_{\delta\alpha_{1,f}} = -55$ m.

On the other hand, there is no significant inclination difference to report between S_1 and S_2, the two satellites lying in the same plane when the deployment ends up.

Remark 6: We target $t = t_f$ osculating parameters that oscillate due to J_2. This implies additional maneuvers of weak magnitude within the strategy, to accurately satisfy the terminal conditions. For instance, Fig. 4 reveals a very small inclination difference caused by some out-of-plane maneuvers. The J_2 effect on the inclination value is corrected this way, so that S_1 and S_2 precisely reach the specified inclination i_f at $t = t_f$.

Finally, Fig. 5 displays a (arbitrarily chosen) satellite S_4 control norm along with its mass time evolution. The graphics are very similar from one satellite to another, and their main point is to confirm the bang-off-bang control structure. We also notice the maneuver locations at both the beginning and end of the deployment. Their duration is so short (approximately two minutes) that they may be considered as quasi-impulsive maneuvers for our application.

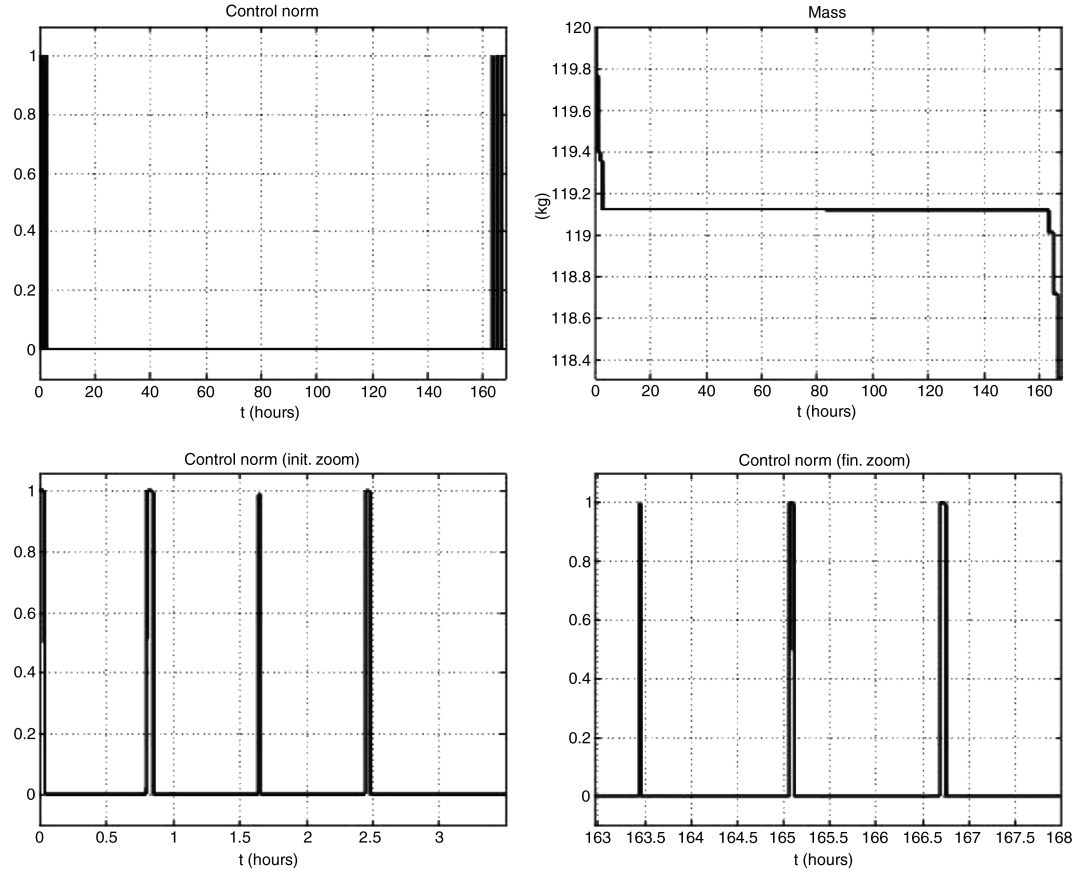

Fig. 5 Time evolution of the control norm and the mass of satellite S_4; global solution.

This shows the robustness of our method based on both optimal control and smoothing approaches. It is not only able to precisely cope with LEO large-sized problems over several weeks and under J_2 influence (see Sec. V.C), but also provides quasi-impulsive maneuver strategies when necessary, which is not its primary purpose.

2. *Example of Alternative Strategy*

a. Preamble. We may think of a competing strategy that would create the drift in Ω between S_2 and S_3, using the J_2 effect combined with a prior semimajor axis difference created by tangential thrusts. In addition, this strategy would involve insignificant out-of-plane maneuvers to counter the oscillating J_2 effect on the inclination, according to Remark 6. This simple strategy is actually not feasible for our application.

Indeed, under the following simplifying assumptions:

1) The maneuvers are impulsive and symmetrically distributed on each satellite.

2) The orbits are assumed to be circular ($e = 0$).

3) The J_2 effects on the semimajor axis, inclination, and true latitude argument are neglected, the difference in Ω secular drift due to J_2 may be expressed up to first order in $(a_3 - a_2)/a_0$.

We may then estimate that for our application parameters, a semimajor axis difference of

$$(a_3 - a_2)_m = \Delta a_{\delta\Omega_{2,f}} = -135 \text{ km} \tag{25}$$

is necessary to obtain the value $\delta\Omega_{2,f} = +0.47$ deg within the seven-day time horizon.

At the same time, the targeted difference in true latitude argument $\alpha_3(t_f) - \alpha_2(t_f) = \delta\alpha_{2,f}[2\pi]$ implies, under the same simplifying assumptions and up to first order in $(a_3 - a_2)/a_0$, that the semimajor axis difference also takes the form

$$(a_3 - a_2)_m = \Delta a_{\delta\alpha_{2,f}} + k\Delta a_{2\pi}, k \in \mathbb{Z} \tag{26}$$

In Eq. (26), $\Delta a_{\delta\alpha_{2,f}}$ is the constant defined in Sec. V.B.1 and $\Delta a_{2\pi}$ is the semimajor axis difference that produces a dephasing of 2π at $t = t_f$.

Conditions (25) and (26) cannot be simultaneously satisfied, except for very specific instances of $\delta\Omega_{2,f}$ and $\delta\alpha_{2,f}$. As a result, complementary out-of-plane maneuvers will be required to reach the specified difference $\delta\Omega_{2,f}$, and "hybrid solutions" (combining both *significant* out-of-plane and tangential thrusts) will be obtained in practice (see Table 1). Each of them may be fully characterized by a value of k, the previous global strategy corresponding to $k = 0$.

b. Effective Strategy. We now present a strategy for which the overall consumption amounts to 7.1 kg through 20 maneuvers.

Figure 6 reveals that a semimajor axis difference $(a_3 - a_2)_m \approx -45$ km was created between satellites S_2 and S_3. This value actually corresponds to $\Delta a_{2\pi}$ in Eq. (26). The latter relation is indeed satisfied, with $k = 1$, the term $\Delta a_{\delta\alpha_{2,f}} = +90$ m being negligible toward $\Delta a_{2\pi}$. Moreover, Fig. 6 confirms that S_2 is shifted from one revolution compared with S_3, because the final difference in true latitude argument is superior to 360 deg.

As for the inclination difference $[(i_3 - i_2)_m = +0.05$ deg], it is, as expected, inferior to the value obtained for the global solution (i.e., $\Delta i_{\delta\Omega_{2,f}} = +0.08$ deg).

The evolution of the remaining parameters being unchanged in comparison with the global solution, the corresponding graphics will not be displayed here.

Remark 7: On a Sun Blade 2500 at 1280 MHz with 2048-MB memory, the computation time required for running the continuation-smoothing method is about 40 minutes (respectively, 1 h) for each local solution and for a deployment over 3.5 days (respectively, seven days). Consequently, the overall CPU time will strongly depend on the number of runs performed by the globalization process (Monte Carlo analysis). The corresponding load may appear important, but it remains acceptable to us because the method is to be used offline for preliminary mission analysis.

C. Evolution of the Global Strategy Versus t_f

Hereafter, we study the influence of the deployment duration on the main features of a given strategy. The so-called global solution in Sec. V.B.1 will be examined for the following values of t_f: 3.5, 7, 14, 16.5, and 19 days.

Remark 8: The upper bound of $t_f = 19$ days follows from the limitations of our material environment (Sun Blade 2500). For longer durations, the J_2 oscillations and the shooting function sensitivity cause prohibitively long computations and sometimes failure of the method.

Figures 7 and 8 display the time evolution of the differential parameters between S_2 and S_3 for $t_f = 3.5$ and 19 days, respectively. The graph shapes are quite similar for intermediate durations t_f, although numerical values may vary.

Let us first look into the semimajor axis difference that allows creating a final dephasing $\delta\alpha_{2,f} = -0.61$ deg. Its average value decreases (from 175 to 40 m) when the deployment duration grows (from $t_f = 3.5$ to 19 days), which is a standard result of space

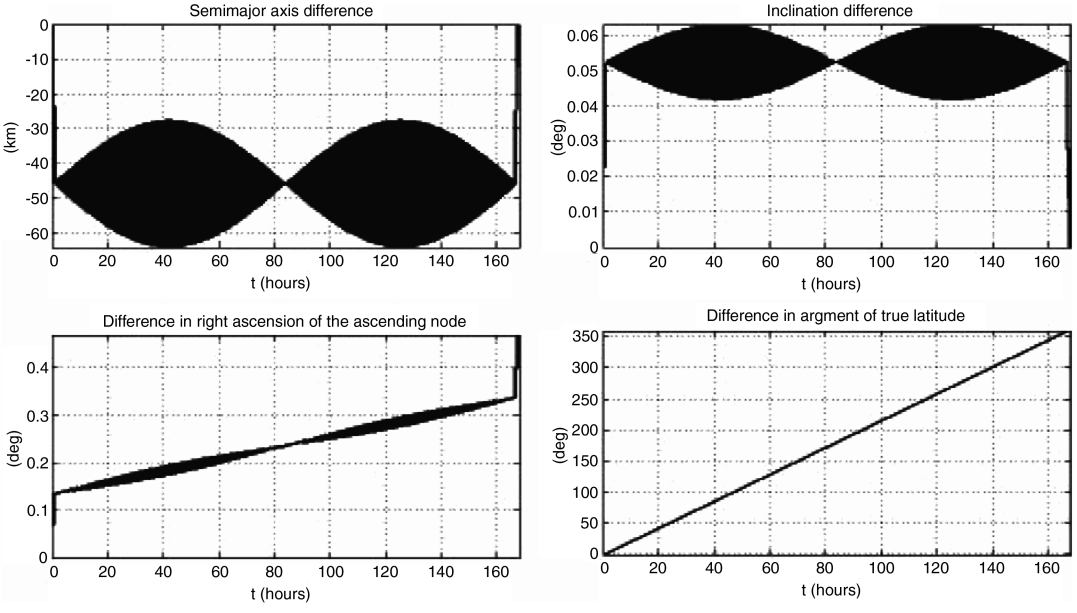

Fig. 6 Time evolution of the differential parameters between satellites S_2 and S_3; local solution.

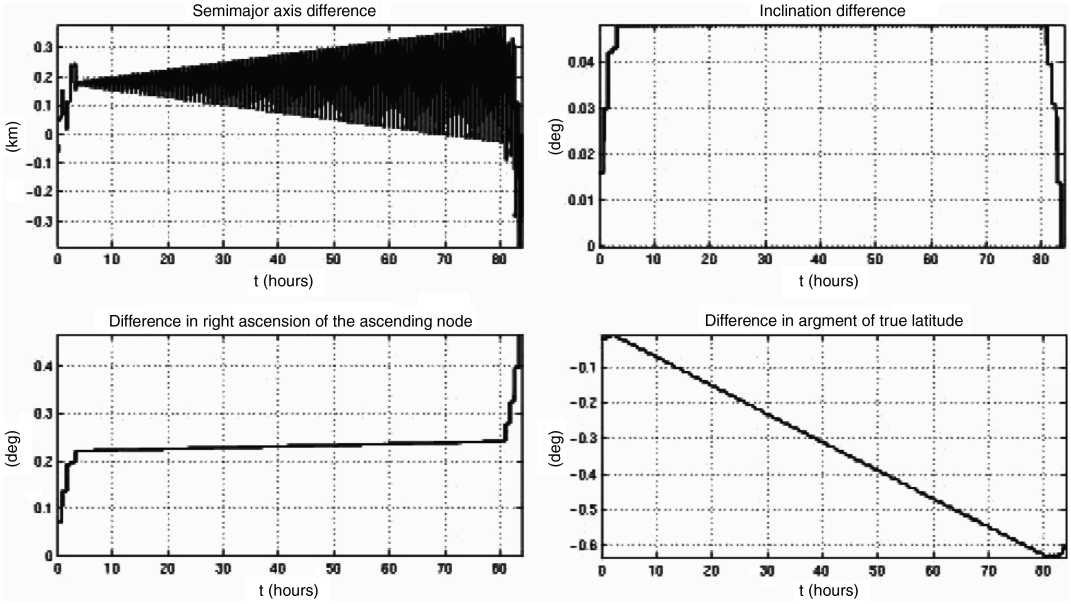

Fig. 7 Time evolution of the differential parameters between S_2 and S_3; global solution; $t_f = 3.5$ days.

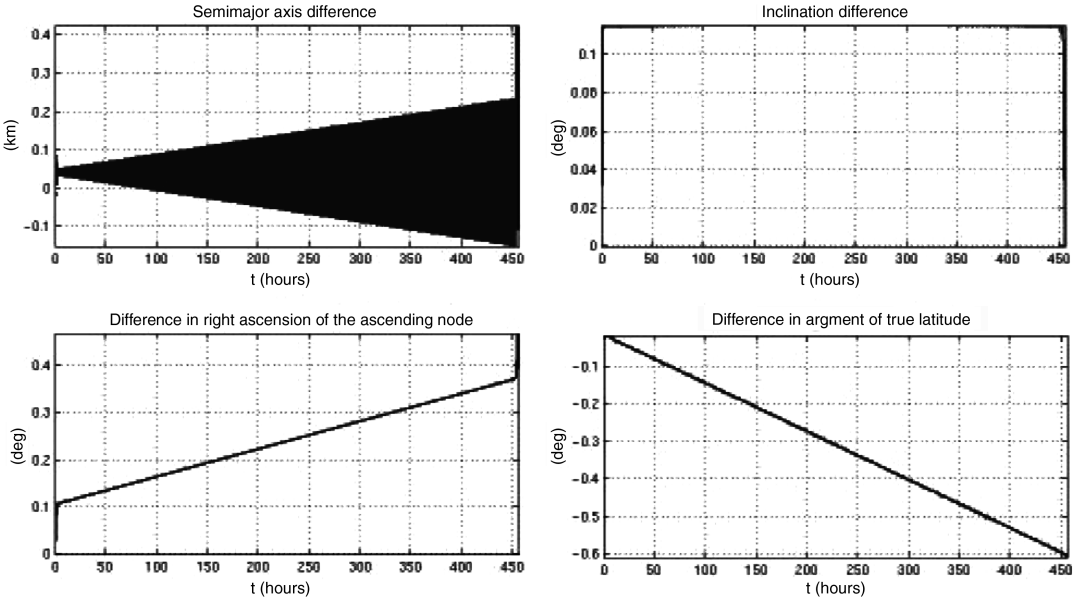

Fig. 8 Time evolution of the differential parameters between S_2 and S_3; global solution; $t_f = 19$ days.

mechanics. We then observe in Figs. 7 and 8 that the drift part (due to J_2) of the difference in Ω ($\delta\Omega_{2,f} = +0.47$ deg) grows as t_f increases. Hence, the central region of the graph associated with $t_f = 3.5$ days is almost flat, whereas for $t_f = 19$ days, the drift effect is predominant over that of thrusts. We finally notice that the inclination difference increases from Fig. 7 (0.048 deg) to Fig. 8 (0.115 deg). However, it will be seen next that $(i_3 - i_2)_m$ is actually not monotonous with respect to t_f.

Table 2 summarizes the average differential parameters that were experimentally read for every tested value of t_f. The semimajor axis and inclination differences are denoted by $(a_3 - a_2)_m$ and $(i_3 - i_2)_m$, respectively. The overall expenditure c is also mentioned. Finally,

$$\frac{(\Omega_3 - \Omega_2)_d}{\delta\Omega_{2,f}} \times 100$$

stands for the differential drift in Ω, expressed as a percentage of the overall difference $\delta\Omega_{2,f}$.

First, the consumption decreases as t_f grows, which tends to show that the optimal strategy increasingly benefits from the J_2 effect. This is confirmed by the evolution of the relative differential drift in Ω, which continuously grows with t_f. Second, we observe that the inclination difference first increases, then stabilizes itself about 0.115 deg for $t_f > 14$ days. Incidentally, the required semimajor axis difference decreases as planned.

Again assuming symmetrically distributed impulsive maneuvers, these observations may be confirmed by analytic computations as soon as the optimal strategy is known.

Remark 9: The role of optimal control techniques is here to provide these strategies with the highest possible accuracy and to handle continuous thrusts when necessary.

In our application, the analytic computations show that the maneuvers take place at two distinct points of true latitude arguments close to $\pi/2$ and $3\pi/2$ for small values of t_f. In this case, the out-of-plane thrusts are exclusively devoted to the creation of an instantaneous difference in Ω (cf. Fig. 7). The reason here is that a too-short deployment duration does not allow taking advantage of the J_2 drift effect.

For larger values of t_f, the maneuvers locations gradually move toward the nodes. In other words, the corresponding thrusts generate

an inclination difference $(i_3 - i_2)_m$ that tends to increase when $t_f < 16.5$ days, then decreases from this value on. It is not easy to analyze this phenomenon because the optimality conditions induce a coupling between both (drift and instantaneous) parts of the difference in Ω. However, we may at least notice that the slope of the differential drift in Ω is obviously bounded by

$$\frac{|\delta\Omega_{2,f}|}{t_f}$$

Because it is also proportional to $(i_3 - i_2)_m$, we have

$$\lim_{t_f \to \infty} (i_3 - i_2)_m = 0$$

Assuming further that the differential values of the orbital parameters remain small toward the corresponding absolute values, our analytic computations yield the following expression of the inclination difference:

$$(i_3 - i_2)_m = \delta\Omega_{2,f} \frac{t_f}{t_f^2 + t_c^2} \tag{27}$$

with

$$t_c = \frac{3R_{\text{eq}}^2 J_2 \sqrt{\mu}}{a_f^{7/2}}$$

and where R_{eq} is the equatorial radius of the terrestrial spheroid, J_2 is the second zonal harmonic, μ is the Earth's gravitational constant, and a_f is the final orbit semimajor axis.

We obtain $t_c = 16.5$ days, as announced. Note also that for $\boldsymbol{t_f = t_c}$, the drift effect is equal to that of thrusts: $\boldsymbol{\delta\Omega_{2,f}/2}$.

Figure 9 draws the theoretical graph of $(i_3 - i_2)_m$ versus t_f (the small circles are from our optimal control tests). This figure illustrates the preceding comments, among them, the decrease of the inclination difference toward zero for $t_f > 16.5$ days. We would probably observe it experimentally for $t_f > 19$ days, but we are not able to carry out those tests (cf. Remark 8).

D. Balanced Strategies

Our balancing process was successfully tested from several critical points of problem (2). The tests have raised the following remarks:

1) The consumption balancing process leads to an increase of the overall fuel expenditure. This tends to indicate that the critical points from which the process was tested are not local maxima of problem (2) (also see Remark 11). Indeed, taking into account the fuel balance constraint to slightly modify a given local solution restricts the feasibility domain of problem (2). Then, if we were in the vicinity of a local maximum, this process would locally decrease the optimal cost function.

2) As $\theta[m_1(t_f), \ldots, m_n(t_f)]$ ranges from θ_0 to $\bar{\theta}$, the deployment strategy stands still, in the sense that the average differential values of the orbital parameters (semimajor axis and eccentricity) stay stable.

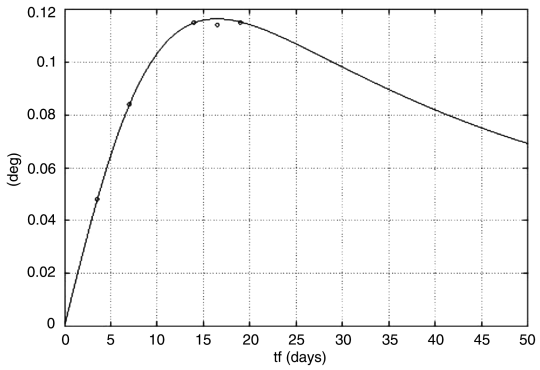

Fig. 9 Evolution of the inclination difference between satellites S_2 and S_3 versus t_f

Conversely, the dates of maneuver and the thrust distributions among the satellites are modified.

3) From any critical point of problem (2) and its corresponding value θ_0 of $\theta[m_1(t_f), \ldots, m_n(t_f)]$, there exists an upper bound of $\theta_1 \in [\theta_0, 1]$, such that for all $\bar{\theta} \in [\theta_0, \theta_1]$, our method locates a solution satisfying $\theta[m_1(t_f), \ldots, m_n(t_f)] = \bar{\theta}$.

Let us now fix $\bar{\theta}$ such that $(1 - \bar{\theta}) = 1.7 \times 10^{-5}$. Then all the critical points in Table 1 (except sol_3) satisfy $\theta[m_1(t_f), \ldots, m_n(t_f)] \geq \bar{\theta}$ and so are also critical points of $P_{\bar{\theta},\geq}$. Our method was implemented to bring sol_3 to $\theta[m_1(t_f), \ldots, m_n(t_f)] = \bar{\theta}$ (similar distribution to that of sol_2). The resulting solution is denoted by sol_{32}.

Table 1 collects the consumption and distribution features of these three strategies, along with the five remaining strategies that were previously obtained. Accordingly, we report the associated overall consumption c, the scalar $(1 - \theta)$ (where θ stands for the value of $\theta[m_1(t_f), \ldots, m_n(t_f)]$ associated with a solution), the maximum difference $\Delta m_{\max}$ among the partial consumptions, and the value $(\Delta m_{\max}/c) \times 100$ expressed as a percentage.

Remark 10: The global strategy (cf. Sec. V.B.2) corresponds to sol_7, and the alternative strategy (cf. Sec. V.B.2) corresponds to sol_5. Most solutions were already balanced from the start ($\theta \approx 1$), which explains why $1 - \theta$ was displayed instead of θ. In addition, this led us to pick a badly balanced solution (sol_3) to illustrate our method.

Using graphics not shown here, it was first confirmed that sol_3 and sol_{32} share common values of the difference in the inclination and semimajor axis. As a consequence, they somehow correspond to the same deployment strategy. Conversely, the distribution $\theta = 0.999983$ for sol_{32} is, as planned, identical to that of sol_2. Incidentally, sol_{32} also coincides with sol_2 in terms of $\Delta m_{\max}/c = 22\%$, which means the same relative maximum consumption gap. As for the absolute gap, it was reduced from 4.06 to 1.88 kg, whereas the overall consumption was raised to 8.72 kg. These results show that one can easily modify the distribution of maneuvers among the satellites to enhance the consumption balance while preserving a given deployment strategy.

Remark 11: All the strategies yielded by our globalization method benefit in a different way from the J_2 effect to reduce the overall fuel consumption. We may then think that they are local minima of the problem, even if we are not able to prove it mathematically. The consumption balancing process has simply shown numerically that the tested strategies were not local maxima. In any case, a large number of solutions are interesting from a mission analysis point of view because they combine an acceptable fuel consumption with a good balance of the consumed masses among the satellites.

VI. Conclusions

An efficient method to compute fuel-optimal nonimpulsive maneuvers was designed here for the deployment of satellite formation flying. Mixing optimal control concepts with smoothing techniques, this approach includes an original and reliable initial phase suitable for the multisatellite framework. In addition, it enables accurately balancing the consumed masses among the satellites, starting from a given solution.

The method was tested against a LEO application involving nonlinear dynamics under J_2 influence. The algorithm behaved well in this numerically tough context by computing several maneuver strategies for deployment over 20 days or so. Seven of them were actually detected, analyzed, and compared for $t_f = 7$ days. This justifies the interest of such a technique when the dates, durations, and directions of thrusts are not known in advance. In addition, it was shown that even impulsive maneuvers might be computed through this approach.

It now remains to further validate the method in some different context, by considering HEO problems, for instance. However, there are many potential applications in mission analysis.

Finally, recall that the collision avoidance is still an open problem for indirect methods. Further investigations are required on this central topic.

Acknowledgment

This work is cofunded by Thales Alenia Space.

References

[1] Hill, G. W., "Researches in the Lunar Theory," *American Journal of Mathematics*, Vol. 1, No. 1, 1878, pp. 5–26. doi:10.2307/2369430

[2] Clohessy, W. H., and Wiltshire, R. S., "Terminal Guidance System for Satellite Rendezvous," *Journal of the Aerospace Sciences*, Vol. 27, No. 9, 1960, pp. 653–658.

[3] Lawden, D. F., *Optimal Trajectories for Space Navigation*, Butterworths, London, 1963, pp. 76–81.

[4] Kim, Y., Mesbahi, M., and Hadaegh, F. Y., "Dual-Spacecraft Formation Flying in Deep Space: Optimal Collision-Free Reconfigurations," *Journal of Guidance, Control, and Dynamics*, Vol. 26, No. 2, 2003, pp. 375–379.

[5] Seo, J. S., and Wiesel, W. E., "Low Thrust Control Optimization for Satellite Formation," *l4th AAS/AIAA Space Flight Mechanics Conference*, American Astronautical Society, Paper AAS 04-256, 2004.

[6] Tillerson, M., and How, J. P., "Formation Flying Control in Eccentric Orbits," AIAA Guidance, Navigation, and Control Conference, Montreal, Canada, AIAA Paper 2001-4092, 2001.

[7] Lim, H.-C., Bang, H.-C., Park, K.-D., and Lee, W.-K., "Optimal Formation Trajectory-Planning Using Parameter Optimization Technique," *Journal of the Astronomy and Space Sciences*, Vol. 21, No. 3, 2004, pp. 209–220.

[8] Junge, O., and Ober-Blobaum, S., "Optimal Reconfiguration of Formation Flying Satellites," *44th IEEE Conference on Decision and Control*, Inst. of Electrical and Electronics Engineers, Piscataway, NJ, 2005, pp. 66–71.

[9] Yang, G., Yang, Q., Kapila, V., Palmer, D., and Vaidyanathan, R., "Fuel Optimal Manoeuvres for Multiple Spacecraft Formation Reconfiguration Using multi-agent Optimization," *International Journal of Robust and Nonlinear Control*, Vol. 12, Nos. 2–3, 2002, pp. 243–283. doi:10.1002/rnc.684

[10] Campbell, M. E., "Planning Algorithm for Multiple Satellite Clusters," *Journal of Guidance, Control, and Dynamics*, Vol. 26, No. 5, 2003, pp. 770–780.

[11] Zanon, D. J., and Campbell, M. E., "Optimal Planner for Spacecraft Formations in Elliptical Orbits," *Journal of Guidance, Control, and Dynamics*, Vol. 29, No. 1, 2006, pp. 171–181.

[12] Garcia, I., and How, J. P., "Trajectory Optimization for Satellite Reconfiguration Maneuvers with Position and Attitude Constraints," *IEEE American Control Conference*, Inst. of Electrical and Electronics Engineers, Piscataway, NJ, 2005, pp. 889–895.

[13] Singh, G., and Hadaegh, F., "Autonomous Path-Planning for Formation Flying Applications," http://trs-new.jpl.nasa.gov/dspace/bitstream/2014/13424/1/01-2358.pdf [retrieved 24 October 2007].

[14] Kim, Y., Mesbahi, M., and Hadaegh, F. Y., "Multiple-Spacecraft Reconfiguration Through Collision Avoidance, Bouncing, and Stalemates," *Journal of Optimization Theory and Applications*, Vol. 122, No. 2, 2004, pp. 323–343. doi:10.1023/B:JOTA.0000042524.57088.8b

[15] Richards, A., How, J. P., Schouwenaars, T., and Feron, E., "Plume Avoidance Maneuver Planning Using Mixed Integer Linear Programming," AIAA Guidance, Navigation, and Control Conference, AIAA Paper 2001-4091, 2001.

[16] Vadali, S. R., Schaub, H., and Alfriend, K. T., "Initial Conditions and Fuel-Optimal Control for Formation Flying of Satellites," AIAA Guidance, Navigation and Control Conference, Portland, OR, AIAA Paper 99-4265, 1999.

[17] Schaub, H., and Alfriend, K. T., "J_2 Invariant Relative Orbits for Spacecraft Formations," *Celestial Mechanics and Dynamical Astronomy*, Vol. 79, No. 2, 2001, pp. 77–95. doi:10.1023/A:1011161811472

[18] Milam, M. B., Petit, N., and Murray, R. M., "Constrained Trajectory Generation for Microsatellite Formation Flying," http://cas.ensmp.fr/~petit/papers/gnc2001/GNC01.pdf [retrieved 24 October 2007].

[19] Guibout, V. M., and Scheeres, D. J., "Spacecraft Formation Dynamics and Design," *Journal of Guidance, Control, and Dynamics*, Vol. 29, No. 1, 2006, pp. 121–133.

[20] Pontryagin, L. S., Boltyansky, V. G., Gamkrelidze, R. V., and Mishchenko, E. F., *The Mathematical Theory of Optimal Processes*, Pergamon, New York, 1964.

[21] Umehara, H., and Mclnnes, C. R., "Fuel-Optimum Near-Miss Avoidance Control for Clustered Satellites," *Proceedings of the 18th International Symposium on Space Flight Dynamics*, ESA SP-548, ESA, Paris, 2004, p. 1093.

[22] Leonard, N., and Fiorelli, E., "Virtual Leaders, Artificial Potentials and Coordinated Control of Groups," *40th IEEE Conference on Decision and Control*, Vol. 3, Inst. of Electrical and Electronics Engineers, Piscataway, NJ, 2001, pp. 2968–2973.

[23] Bertrand, R., and Epenoy, R., "New Smoothing Techniques for Solving Bang-Bang Optimal Control Problems—Numerical Results and Statistical Interpretation," *Optimal Control Applications and Methods*, Vol. 23, No. 4, 2002, pp. 171–197. doi:10.1002/oca.709

[24] Bertrand, R., and Epenoy, R., "Resolution Numérique des Problemes de Commande Optimale a Solution "Bang-Bang" a L'aide de Techniques de Lissage," Centre National d'Etudes Spatiales, Note Technique 147, Paris, 2002.

[25] Bryson, A. E., and Ho, Y. C., *Applied Optimal Control*, Hemisphere, New York, 1975.

[26] Cesari, L., *Optimization Theory and Applications*, Springer–Verlag, New York, 1983.

[27] Powell, M., "A Hybrid Method for Nonlinear Equations," *Numerical Methods for Nonlinear Algebraic Equations*, edited by P. Rabinowitz, Gordon and Breach Science, London, 1970, pp. 87–144.

[28] Dormand, J. R., and Prince, P. J., "Practical Runge–Kutta Processes," *SIAM Journal on Scientific and Statistical Computing*, Vol. 10, No. 5, 1989, pp. 977–989. doi:10.1137/0910057